RESEARCH ACTIVITIES IX
Center for Integrative Bioscience

IX-A Single-Molecule Physiology

A single molecule of protein (or RNA) enzyme acts as a machine which carries out a unique function in cellular activities. To elucidate the mechanisms of various molecular machines, we need to observe closely the behavior of individual molecules, because these machines, unlike man-made machines, operate stochastically and thus cannot be synchronized with each other. By attaching a tag that is huge compared to the size of a molecular machine, or a small tag such as a single fluorophore, we have been able to image the individual behaviors in real time under an optical microscope. Stepping rotation of the central subunit in a single molecule of F_1-ATPase has been videotaped, and now we can discuss its detailed mechanism. RNA polymerase has been shown to be a helical motor that rotates DNA during transcription. Myosin V is another helical motor that moves as a left-handed spiral on the right-handed actin helix. Single-molecule physiology is an emerging field of science in which one closely watches individual, "live" protein/RNA machines at work and examines their responses to external perturbations such as pulling and twisting. I personally believe that molecular machines operate by changing their conformations. Thus, detection of the conformational changes during function is our prime goal. Complementary use of huge and small tags is our major strategy towards this end.

http://www.k2.ims.ac.jp/

IX-A-1 The ATP-Waiting Conformation of Rotating F_1-ATPase Revealed by Single-Pair Fluorescence Resonance Energy Transfer

YASUDA, Ryohei[1]; MASAIKE, Tomoko[2,3]; ADACHI, Kengo; NOJI, Hiroyuki[4]; ITOH, Hiroyasu[5]; KINOSITA, Kazuhiko, Jr.
([1]Cold Spring Harbor Laboratory; [2]ERATO; [3]Tokyo Inst. Tech.; [4]Univ. Tokyo; [5]Hamamatsu Photonics)

[*Proc. Natl. Acad. Sci. U.S.A.* **100**, 9314–9318 (2003)]

F_1-ATPase is an ATP-driven rotary motor in which a rod-shaped γ subunit rotates inside a cylinder made of $\alpha_3\beta_3$ subunits. To elucidate the conformations of rotating F_1, we measured fluorescence resonance energy transfer (FRET) between a donor on one of the three βs and an acceptor on γ in single F_1 molecules. The yield of FRET changed stepwise at low ATP concentrations, reflecting the stepwise rotation of γ. In the ATP-waiting state, the FRET yields indicated a γ position ≈ 40° counterclockwise (= direction of rotation) from that in the crystal structures of mitochondrial F_1, suggesting that the crystal structures mimic a metastable state before product release.

IX-A-2 Single Molecule Imaging of the Rotation of F_1-ATPase

ADACHI, Kengo; NOJI, Hiroyuki[1]; KINOSITA, Kazuhiko, Jr.
([1]Univ. Tokyo)

[*Methods in ENZYMOLOGY* **361**, 211–227 (2003)]

A single molecule of F_1-ATPase has been shown to be a rotary motor, driven by adenosine triphosphate (ATP) hydrolysis, in which the central γ subunit rotates against a surrounding cylinder made of alternately arranged three α and three β subunits. Together with another (yet putative) proton-driven rotary motor F_o, it constitutes the F_oF_1-ATP synthase that synthesizes ATP from adenosine diphosphate (ADP) and inorganic phosphate using proton flow as the energy source. Isolated F_1 composed of $\alpha_3\beta_3\gamma_1\delta_1\varepsilon_1$ subunits only hydrolyzes ATP, and hence is called F_1-ATPase. Its subcomplex $\alpha_3\beta_3\gamma$ suffices for rotation driven by ATP hydrolysis. Single-molecule imaging of this subcomplex has revealed detailed mechanical and kinetic properties of the motor1 activity, and high-resolution atomic structures of F_1 are already available. At present, F_1-ATPase is one of the best characterized molecular motors, or nucleotide-driven molecular machines. It is possible to learn a lot from this rotary machine about the molecular mechanism of chemo-mechanical energy transduction.

Because all molecular machines work stochastically, their operations can never be synchronized with each other in a rigorous sense. Thus, it is necessary to watch the individual behaviors closely. With F_1-ATPase, for example, we have been able to show that it rotates in a unique direction, that it does so in discrete 120° steps, and that 120° steps are resolved into ~ 90° and ~ 30° substeps at low ATP concentrations. We have also been able to measure its rotary torque, and have shown that its energy conversion efficiency can reach ~ 100%. We believe that it would be very difficult, if not impossible, to obtain these results without dealing with individual molecules. Here we describe in detail the techniques involved, hoping that they may also be applicable to other molecular machines, in particular to the detection of conformational changes underlying their function (note that a conformational change accompanies reorientation, or partial rotation, of one part against the other).

For the detection of rotation (or conformational changes), we recommend the complementary use of large and small probes. Here we describe two examples, an actin filament as a probe that is large compared to the rotary motor, and a single fluorophore as a small and

less perturbing probe. We begin with the preparation of materials, and proceed to the setting of functional motor molecules on a glass surface and then to imaging and analysis.

IX-B Bioinorganic Chemistry of Heme-Based Sensor Proteins

Heme-based sensor proteins are a newly recognized class of heme proteins, in which the heme acts as a sensor of gaseous effector molecules such as O_2, NO, and CO. Our research interests focus on the CO-sensing transcriptional activator CooA and the O_2-sensing signal transducer HemAT. We have elucidated the structure and function relationships of CooA and HemAT by mutagenesis and some spectroscopic studies.

IX-B-1 Characterization of the Heme Environmental Structure of Cytoglobin, a Fourth Globin in Humans

SAWAI, Hitomi[1]; KAWADA, Norifumi[1]; YOSHIZATO, Katsutoshi[1]; NAKAJIMA, Hiroshi; AONO, Shigetoshi; SHIRO, Yoshitsugu[1]
([1]RIKEN HARIMA Inst./SPring 8)

[*Biochemistry* **42**, 5133–5142 (2003)]

Cytoglobin (Cgb) represents a fourth member of the globin superfamily in mammals, but its function is unknown. Site-directed mutagenesis, in which six histidine residues were replaced with alanine, was carried out, and the results indicate that the imidazoles of His81 (E7) and His113 (F8) bind to the heme iron as axial ligands in the hexacoordinate and the low-spin state. The optical absorption, resonance Raman, and IR spectral results are consistent with this conclusion. The redox potential measurements revealed an *E*' of 20 mV (*vs* NHE) in the ferric/ferrous couple, indicating that the imidazole ligands of His81 and His113 are electronically neutral. On the basis of the ν(Fe–CO) and ν(C–O) values in the resonance Raman and infrared spectra of the ferrous–CO complexes of Cgb and its mutants, it was found that CO binds to the ferrous iron after the His81 imidazole is dissociated, and three conformers are present in the resultant CO coordination structure. Two are in closed conformations of the heme pocket, in which the bound CO ligand interacts with the dissociated His81 imidazole, while the third is in an open conformation. The ν(Fe–O_2) in the resonance Raman spectra of oxy Cgb can be observed at 572 cm^{-1}, suggesting a polar heme environment. These structural properties of the heme pocket of Cgb are discussed with respect to its proposed *in vivo* oxygen storage function.

IX-B-2 Structure and Function of the CO-Sensor Protein CooA

AONO, Shigetoshi; KOBAYASHI, Katsuaki; INAGAKI, Sayaka

CooA from a photosynthetic bacterium, *R. rubrum*, is the only example of CO-sensor protein so far. We have found a CooA homologue in a thermophilic CO oxidizing bacterium, *Carboxydothermus hydrogenoformans*, and constructed an expression system of CooA from *C. hydrogenoformans* (Ch-CooA) as described below. The gene encoding Ch-CooA was prepared by PCR with a chromosomal DNA of *C. hydrogenoformans* as the template and the two primers (5'-AGG AGA GGA CTA TGG CCA CCC AAA TGA GAT TAA CCG AC-3' and 5'- TTA CTA AAC GCC TGA GGA AAA CTC-3'). The DNA fragment containing *Ch-cooA* was subcloned in pCR4-TOPO vector and then inserted at the EcoRI-site in pKK223-3 vector to construct an expression vector. Ch-CooA was expressed in the soluble fraction of *E. coli* and purified to a homogeneous state by using Q-Sepharose, Hitrap Heparin, and Sephacryl S-100 column chromatography. The purified Ch-CooA showed typical uv/vis spectra for 6-coordinate, low-spin heme proteins. Characterization of the biochemical and biophysical properties of Ch-CooA is now in progress.

IX-B-3 Structure and Function of the Oxygen Sensing Signal Transducer Protein HemAT from *Bacillus subtilis*

AONO, Shigetoshi; KOBAYASHI, Katsuaki; YOSHIMURA, Hideaki

HemAT-Bs is a heme-containing signal transducer protein responsible for aerotaxis of *Bacillus subtilis*. The recombinant HemAT-Bs expressed in *E. coli* is purified as the oxy form in which oxygen is bound to the ferrous heme. HemAT-Bs as isolated gives the Soret, α and β peaks at 414, 578, and 543 nm, respectively. This spectrum is typical of 6-coordinate, low-spin hemoproteins and resembles that of the oxy form of Mb. On deoxygenation with sodium dithionite, HemAT-Bs shows a spectrum with the Soret peak at 431 nm and a single peak at 563 nm in the Q-band region. This spectrum is typical of 5-coordinate, high-spin ferrous hemoproteins, which shows the formation of deoxy HemAT-Bs. CO-bound HemAT-Bs is formed upon the reaction of dithionite reduced HemAT-Bs with CO, which shows the Soret, α and β peaks at 422, 567, and 543 nm, respectively.

HemAT-Bs consists of two domains, *i.e.*, the N-terminal sensor domain that contains a heme and the C-terminal signaling domain. When the C-terminal signaling domain is truncated, the resulting mutants show a different oxygen affinity and a heme environmental structure from those of wild-type HemAT-Bs. These results suggest that a conformational change around the heme pocket is responsible for the intramolecular signal transduction from the sensor domain to the signaling domain.

IX-C Electronic Structure and Reactivity of Active Sites of Metalloproteins

Metalloproteins are a class of biologically important macromolecules that have various functions such as oxygen transport, electron transfer, oxidation, and oxygenation. These diverse functions of metalloproteins have been thought to depend on the ligands from amino acid, coordination structures, and protein structures in immediate vicinity of metal ions. In this project, we are studying the relationship between the structures of the metal active sites and functions of metalloproteins.

IX-C-1 Trigonal Bipyramidal Ferric Aqua Complex with Sterically Hindered Salen Ligand as a Model for Active Site of Protocatechuate 3,4-Dioxygenase

FUJII, Hiroshi; FUNAHASHI, Yasuhiro

[*Angew. Chem., Int. Ed.* **41**, 3638–3641 (2002)]

Protocatechurate 3,4-dioxygenase (3,4-PCD) has been found in soil bacteria and is known to play a role in degrading aromatic molecules in nature. The enzyme is classified as an intradiol dioxygenase and cleaves catechol analogues bound to the iron(III) site into aliphatic products with incorporation of both atoms of molecular oxygen. It has been proposed that the enzyme does not activate an iron-bound oxygen molecule, but rather induces an iron-bound catecholate to react with O_2. Therefore, knowledge of the structure and electronic state of the iron site is essential to understanding the unique reaction of 3,4-PCD. A previous crystalstructu re analysis of 3,4-PCD from Pseudomonas putida revealed a distorted trigonal-bipyramidal ferric iron center with four endogenous protein ligands (Tyr 408, Tyr 447, His 460, and His 462) and a solvent-derived water molecule (see Figure 1). To understand the structure±function relationship of 3,4-PCD, attempts have been made over several decades to prepare inorganic modelcompl exes of 3,4-PCD. However, no iron(III) complex that reproduces the active site of 3,4-PCD has been characterized. We report here the first example of a distorted trigonal-bipyramidal ferric aqua complex with a sterically hindered salen ligand that not only duplicates the active site but also mimics the spectral characteristics of 3,4-PCD.

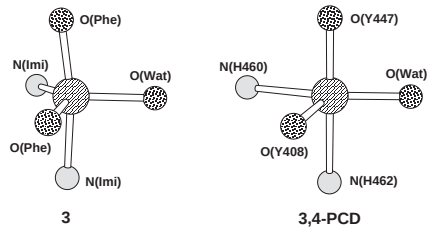

Figure 1. Comparison of Active Site Structures of Our Model Complex and 3,4-PCD.

IX-C-2 An Oxidizing Intermediate Generated from a Salen Iron Complex, Related to the Oxygen Activation by Mononuclear Nonheme Iron Enzymes

KURAHASHI, Takuya; KOBAYASHI, Yoshio[1]; NAGATOMO, Shigenori; KITAGAWA, Teizo; FUJII, Hiroshi
([1]RIKEN)

High-valent iron-oxo species are proposed to be the key reactive intermediate in oxidation reactions catalyzed by the oxygen-activating iron enzyme. In the case of heme enzymes, porphyrin model complexes have been extensively investigated. However, an insight into the nonheme oxidizing intermediate is still limited. Very recently, Wieghardt *et al.* reported the first example of the high-valent iron(IV) species from a nonheme model complex, utilizing the cyclam iron complex. In 2003, Que Jr. *et al.* succeeded in the X-ray crystallographic analysis of the iron(IV) μ-oxo species, using the similar nonheme iron complex. On the other hand, we have been attempting to prepare the nonheme Compound I analog from a salen iron complex. Herein we report the detailed electronic structure and the reactivity of the oxidizing intermediate generated from a salen iron complex and *m*CPBA. To model the monomeric iron center of enzymes, bulky mesityl substituents are introduced to the salen iron complex. Indeed, the aquo complex **1** is found in a monomeric form, due to the steric repulsion by the mesityl group, as already reported. Addition of *m*CPBA to the purple solution of the salen iron complex **1** in dichloromethane at –80 °C produced a blue-green solution (Figure 1). This solution gave a distinct UV-Vis spectrum (λ_{max} = 815 nm) from the starting solution. The intensity of the signal at 815 nm was totally attenuated at room temperature. These results suggest that oxidation of **1** with *m*CPBA generates a transient intermediate having a distinct electronic structure from **1**. The detailed structure of the blue-green intermediate is now being investigated by means of Mössbauer, EPR, NMR and resonance Raman spectroscopy.

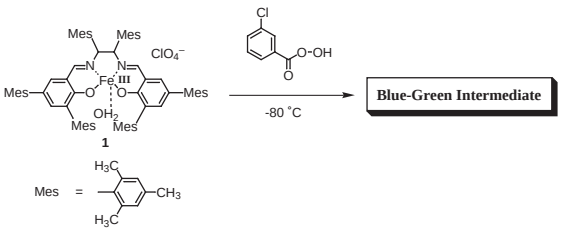

Figure 1. Formation of Blue-Green Intermediate from **1**.

IX-C-3 A Superoxo-Ferrous State in a Reduced Oxy-Ferrous Hemoprotein and Model Compounds

DAVYDOV, Roman[1]; SATTERLEE, James[2]; FUJII, Hiroshi; SAUER-MASARWA, Alexandra[3]; BUSCH, Daryle H.[3]; HOFFMAN, Brian M.[1]
([1]Northwestern Univ.; [2]Washington State Univ.; [3]Univ. Kansas)

[*J. Am. Chem. Soc.* in press]

Cryoreduction of the $[FeO_2]^6$ (n = 6 is the number of electrons in 3*d* orbitals on Fe and π* orbitals on O_2) dioxygen-bound ferroheme through (irradiation at 77 K generates an $[FeO_2]^7$ reduced oxy-heme. Numerous investigations have examined $[FeO_2]^7$ centers that have been characterized as peroxo-ferric centers, denoted $[FeO_2]^7_{per}$, in which a ferriheme binds a dianionic peroxo-ligand. The generation of such an intermediate can be understood heuristically if the $[FeO_2]^6$ parent is viewed as a superoxo-ferric center and the injected electron localizes on the O–O moiety. We here report EPR/ENDOR experiments which show quite different properties for the $[FeO_2]^7$ centers produced by cryoreduction of monomeric oxy-hemoglobin (oxy-GMH3) from *Glycera dibranchiata*, which is unlike mammalian globins in having a leucine in place of the distal histidine, and of frozen aprotic solutions of oxy-ferrous octaethyl porphyrin and of the oxy-ferrous complex of the heme model, cyclidene. These $[FeO_2]^7$ centers are characterized as superoxo-ferrous centers, ($[FeO_2]^7_{sup}$), with nearly unit spin density localized on a superoxo moiety which is end-on coordinated to a low-spin ferrous ion. This assignment is based on their *g* tensors and ^{17}O hyperfine couplings, which are characteristic of the superoxide ion coordinated to a diamagnetic metal ion, and on the absence of detectable endor signals either from the in-plane ^{14}N ligands or from an exchangeable H-bond proton. Such a center would arise if the electron that adds to the $[FeO_2]^6$ superoxo-ferric parent localizes on the Fe ion, to make a superoxo-ferrous moiety. Upon annealing to T > 150 K the $[FeO_2]^7_{sup}$ species recruit a proton and converts to peroxo/hydroperoxo-ferric ($[FeO_2H]^7$) intermediates. These experiments suggest that the primary reduction product is $[FeO_2]^7_{sup}$, and that the internal redox transition to $[FeO_2]^7_{per}/[FeO_2H]^7$ states is driven at least in part by Hbonding/ proton donation by the environment.

IX-C-4 Preparation of Artificial Metalloenzymes by Insertion of Chromium(III) Schiff Base Complexes into Apomyoglobin Mutants

OHASHI, Masataka[1]; KOSHIYAMA, Tomomi[1]; UENO, Takafumi[1]; YAMASE, Manabu[1]; FUJII, Hiroshi; WATANABE, Yoshihito[1]
([1]Nagoya Univ.)

[*Angew. Chem., Int. Ed.* **42**, 1005–1008 (2003)]

Construction of artificial metalloenzymes is one of the most important subjects in bioinorganic chemistry, because metalloenzymes catalyze chemical transformations with high selectivity and reactivity under mild conditions. There are several reports on protein design: introduction of metal binding sites, design of substrate binding cavities, chemical modification of prosthetic groups, and covalent attachment of metal cofactors. In particular, the covalent modification of proteins is a powerful tool for the generation of new metalloenzymes, while the efficiency of the modification is very much dependent on the position and reactivity of the cysteinyl thiol functional group. Herein, we describe a novel strategy for the preparation of artificial metalloenzymes by noncovalent insertion of metal-complex catalysts into protein cavities. The resulting semisynthetic metalloenzymes, apo-myoglobin (apo-Mb) reconstituted with Cr(III) Schiff base complexes, are able to catalyze enantioselective sulfoxidation.

IX-C-5 ^{63}Cu Study of Copper(I) Carbonyl Complexes with Various Tridentate Ligands

KUJIME, Masato; FUJII, Hiroshi

Copper is an essential trace element that plays an important role in a variety of biological functions. We have been studying coordination chemistry of copper complexes ligated by various tridentate ligands as synthetic models for the active site of copper protein which has three imidazolyl groups involved in the histidine residues. Previously we found that the copper(I) carbonyl complexes bearing hydrotris-(pyrazolyl)borates (TPB) exhibit the sharp ^{63}Cu NMR signal in contrast to the other CuL_3L' type complexes, and these chemical shifts were found to be related to the electron donating or withdrawing capabilities of TPB as supported by the dependence of the C≡O stretching vibration. The other copper(I) carbonyl complexes with a series of triazacyclononanes (TACN), tris(4-imidazolyl)carbinols (TIC), trispyrazolylmethanes (TPM), and tris(2-pyridyl)carbomethoxide (TPC) also have shown the good correlations between the δ(^{63}Cu) and C≡O stretching vibration as observed in the TPB system (Figure 1). On the other hand, no meaningful differences were observed for δ(^{13}C) of coordinating carbon monoxide for each complexes, which appears in narrow range around 175 ppm from TMS. These results shows that δ(^{63}Cu) is the sensitive sensor of the extent of back-donation of the Cu-*d* electrons to the antibonding C≡O orbitals, *i.e.*, electron density at the metal center affected by the tridentate ligands. This study also shows the possibility that ^{63}Cu NMR can be the useful tool for the investigation of copper proteins.

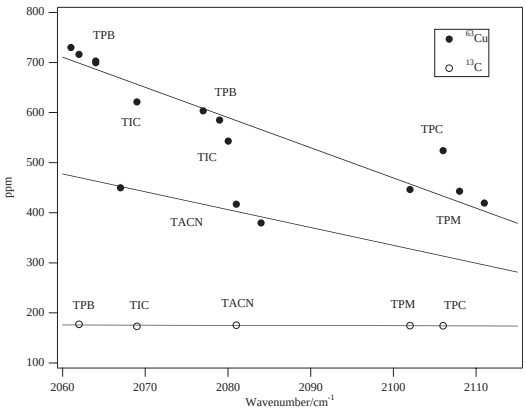

Figure 1. Electronic Effect of Tridentate Ligand on ^{63}Cu- and ^{13}C-NMR Signals of Copper(I) Carbonyl Complexes.

IX-D Molecular Mechanism of Heme Degradation and Oxygen Activation by Heme Oxygenase

Heme oxygenase (HO), an amphipathic microsomal proteins, catalyzes the regiospecific oxidative degradation of iron protoporphyrinIX (heme) to biliverdinIXa, carbon monoxide, and iron in the presence of NADPH-cytochrome P-450 reductase, which functions as an electron donor. Heme oxygenase reaction is the biosynthesis processes of bile pigments and CO, which is a possible physiological messenger. Recent development in the bacterial expression of a soluble form of heme oxygenase has made it possible to prepare in the large quantities for structural studies. In this project, we are studying the molecular mechanism of heme degradation and the oxygen activation by heme oxygenase using various spectroscopic methods.

IX-D-1 Regiospecificity of Each of the Three Steps of Heme Oxygenase Reaction from Hemin to *meso*-Hydroxyhemin, from *meso*-Hydroxyhemin to Verdoheme, and from Verdoheme to Biliverdin

ZHANG, Xuhong[1]; FUJII, Hiroshi; MANSFIELD-MATERA, Kathryn[2]; MIGITA, Catharina Taiko[2]; SUN, Danyu[1]; SATO, Michihiko[1]; IKEDA-SAITO, Masao[2]; YOSHIDA, Tadashi[1]
([1]Yamagata Univ.; [2]Tohoku Univ.)

[*Biochemistry* **42**, 7418–7426 (2003)]

Heme oxygenase catalyzes the regiospecific oxidation of hemin to biliverdin IXα with concomitant liberation of CO and iron by three sequential monooxygenase reactions. The α-regioselectivity of heme oxygenase has been thought to result from the regioselective oxygenation of the heme α-*meso* position at the first step, which leads to the reaction pathway *via meso*-hydroxyheme IXα and verdoheme IXα intermediates. However, recent reports concerning heme oxygenase forming biliverdin isomers other than biliverdin IXα raise a question whether heme oxygenase can degrade *meso*-hydroxyhemin and verdoheme isomers other than the α-isomers. In this paper, we investigated the stereoselectivity of each of the two reaction steps from *meso*-hydroxyhemin to verdoheme and verdoheme to biliverdin, by using a truncated form of rat heme oxygenase-1 and the chemically synthesized four isomers of *meso*-hydroxyhemin and verdoheme. Heme oxygenase-1 converted all four isomers of *meso*-hydroxyhemin to the corresponding isomers of verdoheme. In contrast, only verdoheme IXα was converted to the corresponding biliverdin IXα. We conclude that the third step, but not the second, is stereoselective for the α-isomer substrate. The present findings on regioselectivities of the second and the third steps have been discussed on the basis of the oxygen activation mechanisms of these steps.

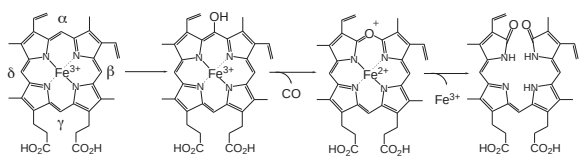

Figure 1. α-Regioselective Heme Catabolism by Heme oxygenase.

IX-E Biomolecular Science

Elucidation of a structure-function relationship of metalloproteins and structural chemistry of amyloid are current subjects of this group. The primary technique used for the first project is the stationary and time-resolved resonance Raman spectroscopy excited by visible and UV lasers. IR-microscope dichroism analysis and AFM are the main techniques for the second project. The practical themes that we want to explore for the first project are (1) mechanism of oxygen activation by enzymes, (2) mechanism of active proton translocation and its coupling with electron transfer, (3) structural mechanism of signal sensing and transduction by heme-based sensor proteins, (4) higher order protein structures and their dynamics, and (5) reactions of biological NO. In category (1), we have examined a variety of terminal oxidases, cytochrome P450s, and peroxidases, and also treated their enzymatic reaction intermediates by using the mixed flow transient Raman apparatus and the Raman/absorption simultaneous measurement device. For (2) the third-generation UV resonance Raman (UVRR) spectrometer was constructed and we are going to apply it to a giant protein like cytochrome *c* oxidase. Recently, we succeeded in pursuing protein folding of apomyoglobin by combining UV time-resolved Raman and rapid mixing device. We also determined the carboxylic side chains of bovine cytochrome oxidase which undergo protonation/deprotonation changes and hydrogen-bonding status changes in response with electron transfers between metal centers or ligand dissociation from heme a_3. Currently, we focus our attention on detecting tyrosine radical for the P intermediate of terminal oxidases. Some positive evidence was obtained for cytochrome *bo*. In (3) we are interested in a mechanism of ligand recognition specific to CO, NO or O_2 and communication pathway of the ligand binding information to the functional part of the protein. For (4) we developed a novel technique for UV resonance Raman measuremnts based on the combination of the first/second order dispersions of gratings and applied it successfully to 235-nm excited RR spectra of several proteins including mutant hemoglobins and myoglobins. Nowadays we can carry out time-resolved UVRR experiments with nanosecond resolution to discuss protein dynamics. With the newly developed third generation UV Raman spectrometer, we have succeeded in isolating the spectrum of tyrosinate in ferric Hb M Iwate, which was protonated in the ferrous state, and the deprotonated state of Tyr244 of bovine cytochrome *c* oxidase. As a model of Tyr244, an imidazole-bound *para*-cresol was synthesized and its UV resonance Raman was investigated. For (5) we purified soluble guanylate cyclase from bovine lung and observed its RR spectra. To further investigate it, we are developing an expression system of this protein. For the amyloid study, we examined FTIR spectra of β_2-microglobulin and its #11-21 peptides which form a core part of amyloid fibril.

IX-E-1 FTIR Detection of Protonation/Deprotonation of Key Carboxyl Side Chains Caused by Redox Change of the Cu_A-Heme *a* Moiety and Ligand Dissociation from the Heme a_3-Cu_B Center of Bovine Heart Cytochrome *c* Oxidase

OKUNO, Daichi[1]; IWASE, Tadashi; SHINZAWA-ITOH, Kyoko[2]; YOSHIKAWA, Shinya[2]; KITAGAWA, Teizo
([1]GUAS; [2]Himeji Inst. Tech.)

[*J. Am. Chem. Soc.* **125**, 7209–7218 (2003)]

FTIR spectral changes of bovine cytochrome *c* oxidase (CcO) upon ligand dissociation from heme a_3 and redox change of the Cu_A-heme *a* moiety (Cu_AFe_a) were investigated. In a photosteady state under CW laser illumination at 590 nm to carbonmonoxy CcO (CcO–CO), the C–O stretching bands due to $Fe_{a3}^{2+}CO$ and $Cu_B^{1+}CO$ were identified at 1963 and 2063 cm^{-1}, respectively, for the fully reduced (FR) state [$(Cu_AFe_a)^{3+}Fe_{a3}^{2+}Cu_B^{1+}$] and at 1965 and 2061 cm^{-1} for the mixed valence (MV) state [$(Cu_AFe_a)^{5+}Fe_{a3}^{2+}$-$Cu_B^{1+}$] in H_2O as well as in D_2O. For the MV state, however, another band due to $Cu_B^{1+}CO$ was found at 2040 cm^{-1}, which was distinct from the α/β conformers in the spectral behaviors, and therefore was assigned to the $(Cu_AFe_a)^{4+}Fe_{a3}^{3+}Cu_B^{1+}CO$ generated by back electron transfer. The FR-minus-oxidized difference spectrum in the carboxyl stretching region provided two negative bands at 1749 and 1737 cm^{-1} in H_2O, which were apparently merged into a single band with a band center at 1741 cm^{-1} in D_2O. Comparison of these spectra with those of bacterial enzymes suggests that the 1749 and 1737 cm^{-1} bands are due to COOH groups of Glu242 and Asp51, respectively. A similar difference spectrum of the carboxyl stretching region was also obtained between $(Cu_AFe_a)^{3+}Fe_{a3}^{2+}Cu_B^{1+}CO$ and $(Cu_AFe_a)^{5+}Fe_{a3}^{2+}Cu_B^{1+}CO$. The results indicate that an oxidation state of the (Cu_AFe_a) moiety determines the carboxyl stretching spectra. On the other hand, CO-dissociated minus CO-bound difference spectra in the FR state gave rise to a positive and a negative peaks at 1749 and 1741 cm^{-1}, respectively, in H_2O, but mainly a negative peak at 1735 cm^{-1} in D_2O. It was confirmed that the absence of a positive peak is not caused by slow deuteration of protein. The corresponding difference spectrum in the MV state showed a significantly weaker positive peak at 1749 cm^{-1} and an intense negative peak at 1741 cm^{-1} (1737 cm^{-1} in D_2O). The spectral difference between the FR and MV states is explained satisfactorily by the spectral change induced by the electron back flow upon CO dissociation as described above. Thus, the changes of carboxyl stretching bands induced both by oxidation of (Cu_AFe_a) and dissociation of CO appear at similar frequencies (~ 1749 cm^{-1}) but are ascribed to different carboxyl side chains.

IX-E-2 Core Structure of Amyloid Fibril Proposed from IR-Microscope Linear Dichroism

HIRAMATSU, Hirotsugu; GOTO, Yuji[1]; NAIKI,

Hironobu[2]; KITAGAWA, Teizo
([1]Osaka Univ.; [2]Fukui Medical Univ.)

[*J. Am. Chem. Soc.* submitted (2003)]

A new approach for studying a peptide conformation of amyloid fibril has been developed. It is based on infrared linear dichroism analysis using an IR-microscope for aligned amyloid fibril. The polarization directions of amide I and II bands were perpendicular similarly for β_2-microglobulin and its #21-31 peptide. Furthermore, this approach has shown that the #21-31 peptide consists of two C=O bonds in the β-sheet that makes 0° with the fibril axis, three C=O bonds in the β-sheet inclined by 27° with respect to the fibril axis, four residues in the random coil by 47°, and two residues in possible β-bulge structure by 32°. Plausible structures of the amyloid core in the fibril is proposed by taking account of these results.

IX-E-3 Resonance Raman Characterization of the P Intermediate in the Reaction of Bovine Cytochrome *c* Oxidase

OGURA, Takeshi[1]; KITAGAWA, Teizo
([1]Himeji Inst. Tech.)

[*Biochim. Biophys. Acta* in press (2003)]

Reduced cytochrome *c* oxidase binds molecular oxygen, yielding an oxygenated intermediate first (Oxy) and then converts it to water *via* the reaction intermediates of P, F, and O in the order of appearance. We have determined the iron-oxygen stretching frequencies for all the intermediates by using time-resolved resonance Raman spectroscopy. The bound dioxygen in Oxy does not form a bridged structure with Cu_B and the rate of the reaction from Oxy to P (P_R) is slower at higher pH in the pH range between 6.8 and 8.0. It was established that the P intermediate has an oxo-heme and definitely not the Fe_{a3}–O–O–Cu_B peroxy bridged structure. The Fe_{a3}=O stretching ($\nu_{Fe=O}$) frequency of the P_R intermediate, 804/764 cm^{-1} for $^{16}O/^{18}O$, is distinctly higher than that of F intermediate, 785/750 cm^{-1}. The rate of reaction from P to F in D_2O solution is evidently slower than that in H_2O solution, implicating the coupling of the electron transfer with vector proton transfer in this process. The P intermediate (607 nm form) generated in the reaction of oxidized enzyme with H_2O_2 gave the $\nu_{Fe=O}$ band at 803/769 cm^{-1} for $H_2{}^{16}O_2$/$H_2{}^{18}O_2$ and the simultaneously measured absorption spectrum exhibited the difference peak at 607 nm. Reaction of the mixed valence CO adduct with O_2 provided the P intermediate (P_M) giving rise to an absorption peak at 607 nm and the $\nu_{Fe=O}$ bands at 804/768 cm^{-1}. Thus, three kinds of P intermediates are considered to have the same oxo-heme a_3 structure. The ν_4 and ν_2 modes of heme a_3 of the P intermediate were identified at 1377 and 1591 cm^{-1}, respectively. The Raman excitation profiles of the $\nu_{Fe=O}$ bands were different between P and F. These observations may mean the formation of a π cation radical of porphyrin macrocycle in P.

IX-E-4 Heme Strctures of Five Hemoglobin Ms Probed by Resonance Raman Spectroscopy

JIN, Yayoi[1]; NAGAI, Masako[1]; NAGAI, Yukifumi[1]; NAGATOMO, Shigenori; KITAGAWA, Teizo
([1]Kanazawa Univ.)

[*Biochemmistry* submitted (2003)]

The α-abnormal Hb Ms show physiological properties different from the β-abnormal Hb Ms, that is, extremely low oxygen affinity of the normal subunit and extraordinary resistance to both enzymatic and chemical reduction of the abnormal met-subunit. In order to get insight into contribution of the heme structure to these differences among Hb Ms, we examined the 406.7-nm excited resonance Raman (RR) spectra of five Hb Ms in the frequency region from 1700 to 200 cm^{-1}, which afford some essential information on the heme structure. The spectra of the abnormal met-subunit in the high frequency region were extracted by the difference calculations between the spectra of the fully-met Hb Ms and of metHb A to eliminate overlaps of the RR bands of the fully-met Hb Ms with those of normal met-subunits. For the half-met Hb Ms (abnormal subunits in the met-form and normal subunits in the deoxy-form), RR bands due to abnormal met-subunits could be clearly distinguished from those of normal deoxy-subunits except for ν_7. In the high frequency region, profound differences between met-α abnormal subunits and met-β abnormal subunits were observed for the in-plane skeletal mode (the $\nu_{C=C}$, ν_{37}, ν_2, ν_{11} and ν_{38} bands), probably reflecting different distortion of the heme structure by the displacement of the heme iron due to tyrosine coordination. Below 900 cm^{-1}, Hb M Iwate (αF8-Tyr) exhibited a distinct spectral pattern for ν_{15}, γ_{11}, $\delta(C_bC_aC_b)_{2,4}$, and $\delta(C_bC_cC_d)_{6,7}$ compared to that of Hb M Boston (αE7-Tyr), although both heme irons are coordinated by Tyr. The β-abnormal Hb Ms, namely, Hb M Hyde Park (βF8-Tyr), Hb M Saskatoon (βE7-Tyr) and Hb M Milwaukee (βE11-Glu), displayed RR band patterns similar to that of metHb A, but with some minor individual differences. The RR bands characteristic of the met-subunits of Hb Ms totally disappeared by chemical reduction and the ferrous heme of abnormal subunits was no more bonded with Tyr or Glu. They were bound to the distal (E7) or proximal (F8) His, and this was confirmed by the presence of the $\nu_{Fe–His}$ mode at 215 cm^{-1} in the 441.6-nm excited RR spectra. A possible involvement of heme distortion in differences of reducibility of abnormal subunits and oxygen affinity of normal subunits is discussed.

IX-E-5 Heme-Regulated Eukaryotic Initiation Factor 2a Kinase (HRI) Activation by Nitric Oxide Is Induced by Formation of Five-Coordinated NO-Heme Complex: Optical Absorption, Electron Spin Resonance and Resonance Raman Spectral Studies

IGARASHI, Jotaro[1]; SATO, Akira; KITAGAWA, Teizo; YOSHIMURA, Tetsuhiko[2]; YAMAUCHI, Seigo[1]; SAGAMI, Ikuko[1]; SHIMIZU, Toru[1]
([1]Tohoku Univ.; [2]Yamagata Public Co. Develop. Ind.)

[*J. Biol. Chem.* submitted (2003)]

Heme-regulated eukaryotic initiation factor 2a (eIF2a) kinase (HRI) regulates the synthesis of hemoglobin in reticulocytes in response to heme availability. HRI has tightly bound heme at the N-terminal domain. Nitric oxide (NO) has been reported to regulate HRI catalysis, but its mechanism remains unclear. In the present study, we examined *in vitro* kinase assay, optical absorption, electron spin resonance (ESR) and resonance Raman spectra of full-length HRI to elucidate regulation mechanism by NO. HRI was activated *via* heme upon NO binding and the Fe(II)HRI(NO) complex had 5-fold eIF2a kinase activity compared to the Fe(III)HRI complex. The Fe(III)HRI complex had Soret peak at 415 nm and exhibited a rhombic ESR signal with *g* values of 2.49, 2.28 and 1.87, suggesting that the Fe(III)HRI complex would be coordinated with His and Cys as axial ligands. Upon addition of NO to the Fe(II)HRI complex, the Soret peak shifted from 423 nm to 398 nm, indicating formation of 5-coordinate NO-heme complex. ESR spectra of the Fe(II)HRI(NO) complex showed a hyperfine triplet, characteristic of 5-coordinate NO-heme complex. Resonance Raman studies showed that Fe–NO and N–O stretching frequencies were located at 527 and 1677 cm^{-1}, respectively in the Fe(II)HRI(NO) complex and that Fe–His stretching frequency was observed at 219 cm^{-1}, immediately after photolysis from the Fe(II)HRI(CO) complex. The spectral findings obtained with full-length HRI were totally different from those obtained with the isolated N-terminal heme-binding domain. We will discuss roles of NO and heme in catalysis with HRI, taking account of heme-based sensor proteins.

IX-E-6 Structural and Spectroscopic Features of a *cis* (Hydroxo)-Fe^{III}-(Carboxylato) Configuration as an Active Site Model for Lipoxygenases

OGO, Seiji[1]; YAMAHARA, Ryo[2]; ROACH, Mark; SUENOBU, Tomoyoshi[3]; AKI, Michihiko; OGURA, Takashi[4]; KITAGAWA, Teizo; MASUDA, Hideki[5]; FUKUZUMI, Shunichi[3]; WATANABE, Yoshihito[6]
([1]IMS and Osaka Univ.; [2]Osaka Univ. and Nagoya Inst. Tech.; [3]Osaka Univ.; [4]Univ. Tokyo; [5]Nagoya Inst. Tech.; [6]Nagoya Univ.)

[*Inorg. Chem.* **41**, 5513–5520 (2002)]

In our preliminary communication (Ogo, S.; Wada, S.; Watanabe, Y.; Iwase, M.; Wada, A.; Harata, M.; Jitsukawa, K.; Masuda, H.; Einaga, H. *Angew. Chem., Int. Ed.* **37**, 2102–2104 (1998)), we reported the first example of X-ray analysis of a mononuclear six-coordinate (hydroxo)iron(III) non-heme complex, $[Fe^{III}(tnpa)(OH)(RCO_2)]ClO_4$ [tnpa = tris(6-neopentylamino-2-pyridylmethyl)amine; for **1**, R = C_6H_5], which has a characteristic *cis* (hydroxo)-Fe^{III}-(carboxylato) configuration that models the *cis* (hydroxo)-Fe^{III}-(carboxylato) moiety of the proposed (hydroxo)iron(III) species of lipoxygenases. In this full account, we report structural and spectroscopic characterization of the *cis* (hydroxo)-Fe^{III}-(carboxylato) configuration by extending the model complexes from **1** to $[Fe^{III}(tnpa)(OH)(RCO_2)]ClO_4$ (**2**, R = CH_3; **3**, R = H) whose *cis* (hydroxo)-Fe^{III}-(carboxylato) moieties are isotopically labeled by $^{18}OH^-$, $^{16}OD^-$, $^{18}OD^-$, $^{12}CH_3{}^{12}C^{18}O_2^-$, $^{12}CH_3{}^{13}C^{16}O_2^-$, $^{13}CH_3{}^{12}C^{16}O_2^-$, $^{13}CH_3{}^{13}C^{16}O_2^-$, and $H^{13}C^{16}O_2^-$. Complexes **1**–**3** are characterized by X-ray analysis, IR, EPR, and UV-vis spectroscopy, and electrospray ionization mass spectrometry (ESI-MS).

IX-E-7 Low-Temperature Stopped-Flow Studies on the Reactions of Copper(II) Complexes and H_2O_2: The First Detection of a Mononuclear Copper(II)-Peroxo Intermediate

OSAKO, Takao[1]; NAGATOMO, Shigenori; TACHI, Yoshimitsu[1]; KITAGAWA, Teizo; ITOH, Shinobu[1]
([1]Osaka City Univ.)

[*Angew. Chem., Int. Ed.* **41**, 4325–4328 (2002)]

Mononuclear copper-active oxygen complexes are key reactive intermediates in many biological and catalytic oxidation processes, but no information is presently available from model systems about mononuclear Cu^{II}-peroxo species. Herein, low-temperature stopped-flow studies are described for the reactions of copper(II) complexes supported by tridentate ligands (L1 and L2) with H_2O_2 to demonstrate that a mononuclear Cu^{II}-peroxo complex is generated from an initially formed Cu^{II}-hydroperoxo intermediate [Equations. (2) and (3)]. The results represent the first example of the direct detection of a mononuclear Cu^{II}-peroxo complex, which provides important information about the reactive intermediates involved in biological and industrial oxidation processes.

$$H_2O_2 + Et_3N \underset{}{\overset{K_1}{\rightleftharpoons}} HO_2^- Et_3NH^+ \quad (1)$$

$$[LCu^{II}]^{2+} + HO_2^- Et_3NH^+ \xrightarrow{k_1} [LCu^{II}\text{-}OOH] + Et_3NH^+ \quad (2)$$
(A)

$$LCu^{II}\text{-}OOH \xrightarrow{k_2} LCu^{II}(O_2) \xrightarrow{k_3[Cu^{II}(L)]} LCu^{II}(O_2)Cu^{II}L \quad (3)$$
(A) (B) (C)

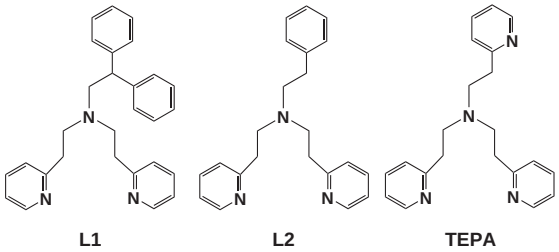

Figure 1.

IX-E-8 Ligand Effect on Reversible Conversion between Copper(I) and Bis(μ-oxo)Dicopper(III) Complex with a Sterically Hindered Tetradentate Tripodal Ligand and Monooxygenae Activity of Bis(μ-oxo)Dicopper(III) Complex

MIZUNO, Masayasu[1]; HAYASHI, Hideki[1];

FUJINAMI, Shuhei[1]; NAGATOMO, Shigenori; OTAKE, Shigenori[1]; UOZUMI, Kounosuke[1]; SUZUKI, Masatatsu[1]; KITAGAWA, Teizo
([1]Kanazawa Univ.)

[*Inorg. Chem.* submitted (2003)]

A new sterically hindered tetradentate tripodal ligand (Me_2-etpy) and its deuterated ligand of the methylene hydrogens (d_4-Me_2-etpy) were synthesized, where Me_2-etpy is bis(6-methyl-2-pyridylmethyl)(2-pyridylethyl)amine. Copper(I) complexes $[Cu(Me_2\text{-etpy}$ or $d_4\text{-}Me_2\text{-etpy})]^+$ (**1** and **1**-d_4, respectively) reacted with dioxygen at –80 °C in acetone to give bis(μ-oxo)dicopper(III) complexes $[Cu_2(O)_2(Me_2\text{-etpy}$ or $d_4\text{-}Me_2\text{-etpy})_2]^{2+}$ (**1**-oxo and **1**-d_4-oxo respectively), the latter of which was crystallographically characterized. Unlike a bis(μ-oxo)dicopper(III) complex with a closely related Me_2-tpa ligand having a 2-pyridylmethyl pendant, **1**-oxo possessing a 2-pyridylethyl pendant is not fully formed even under 1 atm of O_2 at –80 °C and is very reactive toward the oxidation of the supporting ligand. **1**-oxo has a regioselective monooxygenase activity toward the methylene group of the supporting ligand to give a *N*-dealkylated ligand in yield ~ 80% based on a dimer and a corresponding aldehyde. The deuterated ligand d_4-Me_2-etpy greatly stabilizes the bis(μ-oxo)dicopper(III) complex **1**-d_4-oxo, indicating that the rate determining step of the *N*-dealkylation is the hydrogen abstraction from the methylene group. The reversible conversion between **1**-d_4 and **1**-d_4-oxo in acetone was observed depending on the temperature and the thermodynamic parameters (ΔH and ΔS) of the equlibrium were determined to be -53 ± 2 kJ mol^{-1} and -187 ± 10 J mol^{-1}K^{-1}, respectively. The effect of the 2-pyridylethyl pendant in comparison with the 2-pyridylmethyl and 6-methyl-2-pyridylmethyl pendants on the physicochemical properties of the copper(I) and bis(μ-oxo)dicopper(III) species is discussed. (X-ray crystallography (Crystal data for **1**·ClO_4: monoclinic, *C2/c*, a = 20.305(4) Å, b = 12.705(2) Å, c = 16.867(3) Å, β = 100.123(4) Å, V = 4283(1) Å^3, Z = 8, R = 0.044 and R_W = 0.064 ($I \geq 0.0\sigma(\boldsymbol{I})$); for **1**-$d_4$-oxo·$ClO_4$: triclinic, *P*1, a = 10.910(4) Å, b = 11.259(4) Å, c = 14.986(5) Å, α = 82.38(2)°, β = 71.48(2)°, γ = 84.69(2)°, V = 1727(1) Å^3, Z = 1, R = 0.118 and R_W = 0.123($I \geq 0.0\sigma(\boldsymbol{I})$); for **1**-OMe·$ClO_4$: monoclinic, $P2_1/c$, a = 11.642(3) Å, b = 16.689(4) Å, c = 12.885(4) Å, β = 97.700(6)°, V = 2480(1) Å^3, Z = 2, R = 0.031 and R_W = 0.040($\boldsymbol{I} \geq 3\sigma(\boldsymbol{I})$)).

IX-E-9 Dinuclear Copper-Dioxygen Intermediates Supported by Polyamine Ligands

TERAMAE, Shinichi[1]; OSAKO, Takao[2]; NAGATOMO, Shigenori; KITAGAWA, Teizo; FUKUZUMI, Shunichi[1]; ITOH, Shinobu[2]
([1]Osaka Univ.; [2]Osaka City Univ.)

[*J. Inorg. Biochem.* submitted (2003)]

Reactivity of the dicopper(I) and dicopper(II) complexes supported by novel polyamine ligands L1 (*N*,*N*'-dibenzyl-*N*-{3-[benzyl-(6-methyl-pyridin-2-ylmethyl)-amino]-propyl}-*N*'-(6-methyl-pyridin-2-ylmethyl)-propane-1,3-diamine) and L2 (*N*-benzyl-*N*-{2-[bis-(6-methyl-pyridin-2-ylmethyl)-amino]-ethyl}-*N*',*N*'-bis-(6-methyl-pyridin-2-ylmethyl)-ethane-1,2-diamine) towards O_2 and H_2O_2, respectively, have been investigated in order to shed light on the ligand effects on Cu_2/O_2 chemistry. The dicopper(I) complex of L1 (**1a**) readily reacted with O_2 in a 2 : 1 ratio at a low temperature (~ –90 °C) in acetone to afford a mixture of (μ-η^2:η^2-peroxo)dicopper(II) and bis(μ-oxo)dicopper(III) complexes. The formation of these two species has been confirmed by the ESR-silence of the solution as well as their characteristic absorption bands in the UV-vis region [λ_{max} = 350 and 510 nm due to the peroxo complex and ~ 400 nm due to the bis(μ-oxo) complex] and the resonance Raman bands at 729 cm^{-1} [$\Delta\nu(^{16}O_2\text{–}^{18}O_2)$ = 38 cm^{-1} due to the peroxo complex] and at 611 and 571 cm^{-1} [$\Delta\nu(^{16}O_2\text{–}^{18}O_2)$ = 22 cm^{-1} and 7 cm^{-1}, respectively, due to the bis(μ-oxo) complex]. The peroxo and bis(μ-oxo) complexes were unstable even at the low temperature, leading to oxidative *N*-dealkylation at the ligand framework. The dicopper(I) complex of L2 (**2a**) also reacted with O_2 to give (μ-hydroxo)-dicopper(II) complex ($\mathbf{2b^{OH}}$) as the product. In this case, however, no active oxygen intermediate was detected even at the low temperature (–94 °C). With respect to the copper(II) complexes, treatment of the (μ-hydroxo)dicopper(II) complex of L1 ($\mathbf{1b^{OH}}$) with an equimolar amount of H_2O_2 in acetone at –80 °C efficiently gave a (μ-1,1-hydroperoxo)dicopper(II) complex, the formation of which has been supported by its ESR-silence, UV-vis (370 and 650 nm) and resonance Raman spectra [881 cm^{-1}; $\Delta\nu(^{16}O_2\text{–}^{18}O_2)$ = 49 cm^{-1}]. The (μ-1,1-hydroperoxo)dicopper(II) intermediate of L1 also decomposed slowly at the low temperature to give similar oxidative *N*-dealkylation products. Kinetic studies on the oxidative *N*-dealkylation reactions have been performed to get insight into the reactivity of the active oxygen intermediates.

IX-F Molecular Mechanism of Photosensory Protein Function, Excitation Energy Transfer and Electron Transfer in Biological Systems

We are interested in photochemistry, photophysics, photoenergy conversion and photosignal transduction in living orgamisms. Above all, the primary interest in our laboratory is the molecular mechanism of photosensory proteins including rhodopsin and photoactive yellow protein. Using theoretical/computational techniques, we study what happens in these photosensory proteins after light illumination and how these proteins convert light energy into conformational changes.

Excitation energy transfer is a significant process in biophysics. The light-harvesting antenna system in photosynthetic purple bacteria collects and transfers photoenergy efficiently by its unique mechanism. We study this mechanism theoretically.

The electron transfer in biological systems is mostly long-range electron transfer that occurs by the electron tunneling through the protein media. Using theoretical/computational methods, we calculate the electron tunneling current in the protein matrix and analyze how intraprotein electron transfer occurs.

IX-F-1 Role of Protein in the Primary Step of the Photoreaction of Yellow Protein

YAMADA, Atushi[1]; ISHIKURA, Takakazu[1]; YAMATO, Takahisa[2]
([1]Nagoya Univ.; [2]IMS and Nagoya Univ.)

[*Proteins: Struct., Funct., Genet.* in press]

We show the unexpectedly important role of the protein environment in the primary step of the photoreaction of the yellow protein after light illumination. The driving force of the *trans*-to-*cis* isomerization reaction was analyzed by a computational method. The force was separated into two different components: the term due to the protein-chromophore interaction and the intrinsic term of the chromophore itself. As a result, we found that the contribution from the interaction term was much greater than that coming from the intrinsic term. This accounts for the efficiency of the isomerization reaction in the protein environment in contrast to that in solution environments. We then analyzed the relaxation process of the chromophore on the excited-state energy surface and compared the process in the protein environment and that in a vacuum. Based on this analysis, we found that the bond-selectivity of the isomerization reaction also comes from the interaction between the chromophore and the protein environment.

IX-F-2 Direct Measure of Functional Importance Visualized Atom-by-Atom for Photoactive Yellow Protein

YAMADA, Atushi[1]; ISHIKURA, Takakazu[1]; YAMATO, Takahisa[2]
([1]Nagoya Univ.; [2]IMS and Nagoya Univ.)

[Proteins: Struct., Funct., Genet. submitted]

Photoreceptor proteins serve as efficient nanomachines for the photoenergy conversion and the photosignal transduction of living organisms. For instance, the photoactive yellow protein derived from a halophilic bacterium has the *p*-coumaric acid chromophore, which undergoes an ultrafast photoisomerization reaction after light illumination. To understand the structure-function relationship at the atomic level, we used a computational method to find *functionally important atoms* for the photoisomerization reaction of the photoactive yellow protein. In the present study, a "direct" measure of the functional significance was quantitatively evaluated for each atom by calculating the *partial atomic driving force* for the photoisomerization reaction. As a result, we revealed the reaction mechanism in which the specific role of each functionally important atom has been well characterized in a systematic manner. In addition, we observed that this mechanism is strongly conserved during the thermal fluctuation of the photoactive yellow protein.

IX-F-3 A Computational Study on the Stability of the Protonated Schiff Base of Retinal in Rhodopsin

YAMADA, Atushi[1]; KAKITANI, Toshiaki[1]; YAMAMOTO, Shigeyoshi[2]; YAMATO, Takahisa[3]
([1]Nagoya Univ.; [2]Chukyo Univ.; [3]IMS and Nagoya Univ.)

[*Chem. Phys. Lett.* **366**, 670–675 (2003)]

We investigated the effect of amino acids in rhodopsin on the protonation state of the Schiff base (SB) retinal. We constructed a model system consisting of SB retinal, Glu113(counterion), and eight residues. For this model, we considered two states of the SB retinal, namely, the protonated/deprotonated state. We then performed *ab initio* MO calculations at the RHF/6-31g* level. As a result, the protonated state was stabler than the deprotonated state. Interestingly, we observed an additive rule for the contribution to the stabilization energy due to each amino acid. Above all, it turned out that Ser186 and Cys187 play a significant role in the stability.

IX-F-4 Destructive Interference in the Electron Tunneling through Protein Media

KAWATSU, Tsutomu[1]; KAKITANI, Toshiaki[2]; YAMATO, Takahisa[3]
([1]Duke Univ.; [2]Nagoya Univ.; [3]IMS and Nagoya Univ.)

[*J. Phys. Chem. B* **106**, 11356–11366 (2002)]

We investigated the origin of the very rapid and large fluctuation of the electron tunneling matrix element T_{DA} due to the thermal fluctuation of protein conformation which was recently observed by the simulation study (Daizadeh, I.; Medvedev, E. S.; Stuchebrukhov, A. A. *Proc. Natl. Acad. Sci. U.S.A.* **94**, 3703 (1997)). We made analysis of this phenomena by using the interatomic tunneling current map of Ru-modified azurins. We defined a new index, degree of destructive interference Q, by making an average of the intermediate level for the interatomic tunneling currents. We found an empirical relation that $|T_{DA}|$ is proportional to Q^{-1} holds true in the course of thermal fluctuation of protein conformation. Comparing maps of the interatomic tunneling currents with different values of Q, we found that the very rapid (in much less than 1 ps) and large amount (maximally 2 orders of magnitude) of fluctuations in T_{DA} are caused by the reconnection and the change in the direction of interatomic tunneling currents with considerable amplitudes. By taking the statistical average for the dynamics effect of $\log|T_{DA}|$, we found that the range of the averaged dynamic modification of electron transfer rate amounts to more than 2 orders of magnitude in the Ru-modified azurins. In the systems with a large range of dynamic modification, this nuclear dynamics effect contributes to enhance the thermally averaged electron transfer rate considerably.

IX-F-5 Unique Mechanism of Excitation Energy Transfer, Electron Transfer and Photoisomerization in Biological Systems

KAKITANI, Toshiaki[1]; KAWATSU, Tsutomu[2]; KIMURA, Akihiro[1]; YAMADA, Atushi[1]; YAMATO, Takahisa[3]; YAMAMOTO, Shigeyoshi[4]
([1]Nagoya Univ.; [2]Duke Univ.; [3]IMS and Nagoya Univ.; [4]Chukyo Univ.)

[*J. Biol. Phys.* **28**, 367–381 (2002)]

We discuss unique mechanisms typical in the elementary processes of biological functions. We focus on three topics. Excitation energy transfer in the light-harvesting antenna systems of photosynthetic bacteria is unique in its structure and the energy transfer mechanism. In the case of LH2 of *Rhodopseudomonas acidophila*, the B850 intra-ring energy transfer and the inter-ring energy transfer between B800 and B850 take place by the intermediate coupling mechanism of energy transfer. The excitonic coherent domain shows a wave-like movement along the ring, and this property is expected to play a significant role in the inter-ring energy transfer between LH2's. The electron transfer in biological systems is mostly long-range electron transfer that occurs by the electron tunneling through the protein media. There is a long-standing problem that which part of protein media is used for the electron tunneling root. As a result of our detailed analysis, we found that the global electron tunneling root is a little winded with a width of a few angstrom, reflecting the property of tertiary and secondary structures of the protein and it is affected by the thermal fluctuation of protein structure. Photoisomerization of rhodopsin is very unique: The *cis-trans* photoisomerization of rhodopsin occurs only around the C11=C12 bond in the counterclockwise direction. Its molecular mechanism is resolved by our MD simulation study using the structure of rhodopsin which was recently obtained by the X-ray crystallographic analysis.

IX-F-6 Analysis of Cis-Trans Photoisomerization Mechanism of Rhodopsin Based on the Tertiary Structure of Rhodopsin

YAMADA, Atushi[1]; YAMATO, Takahisa[2]; KAKITANI, Toshiaki[1]; YAMAMOTO, Shigeyoshi
([1]Nagoya Univ.; [2]IMS and Nagoya Univ.; [3]Chukyo Univ.)

[*J. Photosci.* **9**, 51–54 (2002)]

We propose a novel mechanism (Twist Sharing Mechanism) for the *cis-trans* photoisomerization of rhodopsin, based on the molecular dynamics (MD) simulation study. New things devised in our simulations are (1) the adoption of Mt. Fuji potentials in the excited state for twisting of the three bonds C9=C10, C11=C12 and C13=C14 which are modeled using the detailed ab initio quantum chemical calculations and (2) to use the rhodopsin structure which was resolved recently by the X-ray crystallographic study. As a result, we found the followings: Due to the intramolecular steric hindrance between 20-methyl and 10-H in the retinal chromophore, the C12–C13 and C10–C11 bonds are considerably twisted counterclockwise in rhodopsin, allowing only counterclockwise rotation of the C11=C12 in the excited state. The movement of 19-methyl in rhodopsin is blocked by the surrounding three amino acids, Thr118, Met207 and Tyr268, prohibiting the rotation of C9=C10. As a result only all-*trans* form of the chromophore is obtainable as a photoproduct. At the 90 degrees twisting of C11=C12 in the course of photoisomerization, twisting energies of the other bonds amount to about 20 kcal/mol. If the transition state for the thermal isomerization is assumed to be similar to this structure, the activation energy for the thermal isomerization around C11=C12 in rhodopsin is elevated by about 20 kcal/mol and the thermal isomerization rate is decelerated by 10^{-14} times than that of the retinal chromophore in solution, protecting photosignal from the thermal noise.